

# Fast 2DGS: Efficient Image Representation with Deep Gaussian Prior

Hao Wang<sup>1\*</sup>, Ashish Bastola<sup>1</sup>, Chaoyi Zhou<sup>1</sup>, Wenhui Zhu<sup>2</sup>, Xiwen Chen<sup>1</sup>, Xuanzhao Dong<sup>2</sup>,  
Siyu Huang<sup>1</sup>, and Abolfazl Razi<sup>1</sup>

<sup>1</sup>Clemson University

<sup>2</sup>Arizona State University

{hao9, abastol, chaoyiz, xiwenc, siyuh, arazi}@clemson.edu, {wzhu59, xdong64}@asu.edu

## Abstract

As generative models become increasingly capable of producing high-fidelity visual content, the demand for efficient, interpretable, and editable image representations has grown substantially. Recent advances in 2D Gaussian Splatting (2DGS) have emerged as a promising solution, offering explicit control, high interpretability, and real-time rendering capabilities ( $> 1000$  FPS). However, high-quality 2DGS typically requires post-optimization. Existing methods adopt random or heuristics (e.g., gradient maps), which are often insensitive to image complexity and lead to slow convergence ( $> 10$ s). More recent approaches introduce learnable networks to predict initial Gaussian configurations, but at the cost of increased computational and architectural complexity. To bridge this gap, we present **Fast-2DGS**, a lightweight framework for efficient Gaussian image representation. Specifically, we introduce *Deep Gaussian Prior*, implemented as a conditional network to capture the spatial distribution of Gaussian primitives under different complexities. In addition, we propose an *attribute regression network* to predict dense Gaussian properties. Experiments demonstrate that this disentangled architecture achieves high-quality reconstruction in a single forward pass, followed by minimal fine-tuning. More importantly, our approach significantly reduces computational cost without compromising visual quality, bringing 2DGS closer to industry-ready deployment. Our source code and sample datasets are available at: <https://github.com/Aztech-Lab/Fast-2DGS>

## 1. Introduction

The exponential growth of visual data in the era of Artificial Intelligence Generated Content (AIGC) has reignited the demand for efficient, scalable, and manipulable image representations [34]. In domains such as digital entertainment[4], content creation[14, 40, 42], and

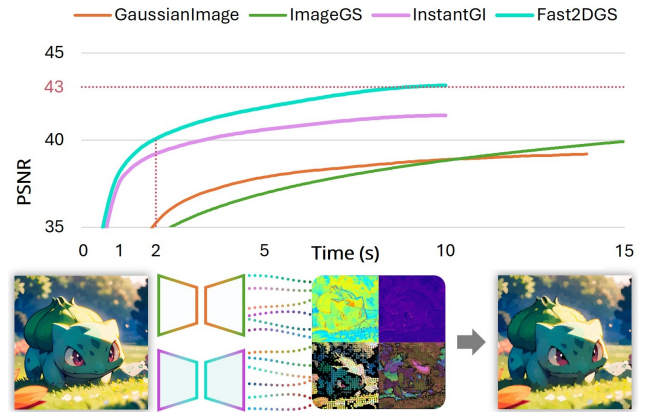


Figure 1. Concept of the proposed Fast 2DGS. We adopt two separate lightweight networks to perform prediction of Gaussian primitives. Our method achieves 40 PSNR in 2 seconds of fine-tuning, and reaches 43 within 10 seconds.

gaming[24], visual data plays a critical role in spatial perception and reasoning[10]. Traditional pixel-based formats (JPEG, PNG)[28], while ubiquitous, suffer from spatial redundancy and lack semantic structure [41]. In contrast, neural representations aim to compress visual signals into deep network parameters or compact primitives [33]. While effective for compression, Implicit Neural Representations (INRs) face significant latency issues [8].

Recently, 2D Gaussian Splatting (2DGS) [39] has been proposed as an explicit alternative. By representing an image as a collection of 2D anisotropic Gaussians explicitly, 2DGS offers fast decoding ( $> 1000$  FPS) using efficient rasterization, and intuitive editability [13, 39, 45]. However, the quality of 2DGS is highly dependent on initialization. For instance, random initialization places primitives uniformly. This forces the optimizer to slowly migrate points to high-frequency regions, requiring  $\sim 10$ k iterations to converge. In contrast, heuristic-based initialization utilizes gradient magnitude or saliency maps [41], while offering improvements over random initialization, these static heuristics are limited in dynamic scenarios[39, 41].

\*Corresponding author

Instant GaussianImage [37] introduced a network-based initialization strategy customized for the 2D Gaussian Splatting task. Instead of relying on iterative optimization from scratch, it employs a neural network as an encoder to predict Gaussian parameters, including spatial locations, covariance structures, and color attributes from the input image. The predicted probability maps (PPM) are converted into discrete Gaussian centers using a dithering-based sampling algorithm[27], enabling adaptive and structure-aware initialization. This hybrid strategy significantly accelerates convergence, reducing encoding time while maintaining high reconstruction quality from the outset. Nevertheless, the design of Instant GaussianImage introduces several practical concerns. Its reliance on feature engineering complicates the Gaussian encoding process, and the heavy network architecture introduces computational overhead. While it performs well in experiments, the increasing complexity and computational cost pose limitations for scalable deployment in industrial applications.

To address these challenges, we present **Fast2DGS**, a framework that transforms Gaussian initialization from a heuristic guess into a learning-based task. Specifically, we introduce Deep Gaussian Prior, where the spatial distribution of Gaussians is learned through an iterative bootstrapping loop. Furthermore, we employ a lightweight UNet for Gaussian feature prediction. By stripping away the feature engineering pipelines, we demonstrate that effective Gaussian attribute prediction does not necessitate elaborate architectural designs, as show in Figure 1. In summary, our contribution is three-fold:

- We propose Deep Gaussian Prior, an initialization strategy learned through an iterative optimization-sampling loop. By simulating the optimization trajectory, our method captures a content-aware distribution that breaks the uniform bias of random initialization, significantly accelerating convergence.
- We present a streamlined framework that anchors Gaussian cardinality ( $K$ ) to compression rates. By employing a lightweight backbone without complex feature engineering, we transform the ill-posed Gaussian allocation into a tractable, batch-parallelizable learning task.
- We demonstrate that our framework achieves superior trade-offs between reconstruction quality, inference latency, and cross-dataset generalizability compared to existing Gaussian image approaches.

## 2. Related Work

### 2.1. Image Representation

Image representation serves as the foundation across various computer vision and signal processing tasks, including image compression[33], super-resolution[2, 17], and generative modeling[3, 14, 40]. Traditionally, images have

been represented via discrete grid-based formats (e.g., pixels) or transform-domain coefficients (e.g., DCT[9, 43], Wavelets[5]). In recent years, Implicit Neural Representations (INRs) have emerged as dominant the deep learning domain by utilizing multilayer perceptrons (MLPs) to parameterize images as continuous functions mapping spatial coordinates to color values [33]. INR models such as SIREN[32], WIRE[30], and COIN++[12] have demonstrated remarkable capabilities in capturing high-frequency details and achieving resolution independence. However, the implicit nature of these methods imposes significant computational bottlenecks [8]. For instance, decoding a single pixel requires a full forward pass through the neural network, resulting in slow inference speeds and substantial GPU memory consumption. Furthermore, implicit models typically function as black boxes and lack efficient support for hardware-friendly random access or local editing.

### 2.2. 2D Gaussian Splatting for Images

Gaussian Splatting (GS) has recently emerged as a powerful tool for 3D scene reconstruction and real-time rendering[20, 44]. Compared to implicit neural representations that rely on MLPs, 3D GS employs explicit 3D Gaussians as representation units, combined with a differentiable tile-based rasterization pipeline[23, 36]. This approach has demonstrated exceptional performance in tasks ranging from SLAM to dynamic scene modeling [21, 35].

Directly applying the 3D GS framework to 2D images introduces significant redundancy and computational inefficiencies as 3D Gaussians typically carry up to 59 parameters (e.g., spherical harmonics for view-dependent color) to ensure multi-view consistency [38], which creates massive storage overhead when representing a single static image [38]. Furthermore, without accurate depth, sorting becomes arbitrary, and the standard  $\alpha$ -blending may prematurely terminate ray marching, leading to the underutilization of Gaussian primitives [39].

To address these challenges, GaussianImage[39] introduced a hardware-level optimization for 2D image representation by removing the need for sorting, allowing for highly parallelized rasterization that achieves decoding speeds of approximately 2000 FPS [39]. However, despite these advancements, significant challenges remain. Specifically, while the inference speed is ultra-fast, the encoding process (fitting) is still orders of magnitude slower than VAE-based approaches [37]. Image-GS [41] then introduced a content-adaptive method to address this inefficiency. Instead of random initialization, it employs gradient-guided sampling to allocate primitives to high-frequency regions and progressively spawns Gaussians in areas with persistent reconstruction errors. While it accelerates the fine-tuning speed, it struggles to model high-frequency pixel-level sensor noise from natural photorealistic

tic images. Instant GaussianImage [37] proposes a generalizable network framework for rapid Gaussian initialization by introducing a learnable Position Probability Map (PPM) supervised by optimal Gaussian density. It achieves high-fidelity reconstruction in a single feedforward pass followed by minimal fine-tuning. However, this sophisticated initialization pipeline requires an intensive triangulation process and additional memory footprint for the feature extraction network.

### 3. Method

#### 3.1. Gaussian Image Rendering

**Gaussian Function.** We represent an image  $I \in \mathbb{R}^{H \times W \times 3}$  using a set of  $K$  2D Gaussian primitives  $\Theta = \{\mathbf{g}_k\}_{k=1}^K$ . Unlike 3DGS approaches, we employ an optimized 2DGS rendering engine from ImageGS [41], where the opacity attribute is omitted as occlusion handling is unnecessary for 2D representation. Thus, each Gaussian primitive is defined by: **Center position**  $\boldsymbol{\mu}_k \in \mathbb{R}^2$ , **Covariance matrix**  $\boldsymbol{\Sigma}_k \in \mathbb{R}^{2 \times 2}$ , and **Color vector**  $\mathbf{c}_k \in \mathbb{R}^3$  (RGB). The spatial influence of the  $k$ -th Gaussian at pixel  $\mathbf{x}$  is then given by:

$$G_k(\mathbf{x}) = \exp\left(-\frac{1}{2}(\mathbf{x} - \boldsymbol{\mu}_k)^T \boldsymbol{\Sigma}_k^{-1} (\mathbf{x} - \boldsymbol{\mu}_k)\right). \quad (1)$$

**Covariance Decomposition.** To maintain the positive semi-definite constraint of  $\boldsymbol{\Sigma}_k$ , we employ the Rotation-Scaling (RS) decomposition from ImageGS [41], as it decouples orientation from extent, which is easier for neural networks to learn:

$$\boldsymbol{\Sigma}_k = \mathbf{R}(\theta_k) \mathbf{S}(s_k) \mathbf{S}(s_k)^T \mathbf{R}(\theta_k)^T, \quad (2)$$

where  $\mathbf{R}(\theta_k) = \begin{bmatrix} \cos \theta_k & -\sin \theta_k \\ \sin \theta_k & \cos \theta_k \end{bmatrix}$  is the rotation matrix and  $\mathbf{S}(s_k) = \text{diag}(s_{x,k}, s_{y,k})$  is the scaling matrix.

**Rendering Model.** We adopt the normalized tile-based rendering model from ImageGS to ensure high-fidelity reconstruction [41]. Since 2D representation does not require depth sorting, the alpha-blending is replaced with a normalized weighted summation, which effectively regularizes the pixel color reconstruction:

$$\hat{I}(\mathbf{x}) = \frac{\sum_{k \in \mathcal{N}(\mathbf{x})} G_k(\mathbf{x}) \cdot \mathbf{c}_k}{\sum_{k \in \mathcal{N}(\mathbf{x})} G_k(\mathbf{x}) + \epsilon}, \quad (3)$$

where  $\mathcal{N}(\mathbf{x})$  denotes the set of relevant Gaussians covering pixel  $\mathbf{x}$  (e.g., top- $K$  filtering), and  $\epsilon$  ensures numerical stability. For convenience, we use

$$\hat{I}(\mathbf{x}) = \sum_{k=1}^K \mathcal{R}(\mathbf{g}_k) = \mathcal{R}(\Theta) \quad (4)$$

to represent the rasterization of  $K$  Gaussians. This formulation remains fully differentiable w.r.t. all parameters  $\Theta$ .

#### 3.2. Regularize ill-Posedness via Sampling

Directly predicting the set  $\Theta$  from an image  $I$  using a neural network is challenging, where a network outputting a fixed-size tensor faces a permutation ambiguity ( $K!$  possible orderings) as  $\Theta$  is unordered [19]. Furthermore, the inverse problem  $\mathcal{R}^{-1}(I)$  is typically ill-posed, as multiple Gaussian configurations can yield identical images (e.g., one large Gaussian vs. many small overlapping ones) [18].

To regularize the search space of this multi-solution problem, we anchor the decomposition to a hard  $K$  (num. of Gaussians) primitives, following the InstantGI[37]. This constrains the search space from a high-dimensional continuous manifold to a structured subspace [22, 25]. Rather than deterministic regression, we formulate position initialization as a sampling process from a learned probability distribution, where deep neural networks can handle naturally [11, 26].

However, bridging the continuous spatial distribution (Heatmap  $\mathcal{H}$ ) and the discrete set of Gaussian positions ( $\mathbf{P} = \{\mu_k\}$ ) introduces a critical bottleneck: the sampling operation  $\mathbf{P} \sim S(\mathcal{H})$  is non-differentiable. As a result, the gradients from the reconstruction loss  $\mathcal{L}_{rec}$  cannot propagate back to update the heatmap:

$$\frac{\partial \mathcal{L}_{rec}}{\partial \mathcal{H}} = \frac{\partial \mathcal{L}_{rec}}{\partial \mathbf{P}} \cdot \underbrace{\frac{\partial \mathbf{P}}{\partial \mathcal{H}}}_{\text{gradient detachment}} \approx 0. \quad (5)$$

This gradient blockage renders standard end-to-end training infeasible and validates the rationale behind multi-stage learning strategies in InstantGI [37]. To overcome this, we decouple the learning process by mapping the discrete, optimized Gaussian positions back into a continuous density field. In other words, we train an individual Gaussian Prior prediction network that approximates the optimal spatial distribution of  $K$  Gaussians.

#### 3.3. Deep Gaussian Prior

While previous works often rely on static heuristics: assuming Gaussian positions strictly follow image gradients or edges [41], we posit that the optimal spatial distribution is non-stationary and governed by the interplay between local spectral density and global optimization dynamics[26].

We define the Gaussian Position Prior as a dense field  $\mathcal{H}$  (heatmap), and we observed that  $\mathcal{H}$  is deeply correlated with the Number of Gaussians ( $K$ ). For instance, in a low-bitrate setting (small  $K$ ), Gaussians  $\Theta = \{\mathbf{g}_k\}_{k=1}^K$  must prioritize global coverage to represent the base structure, whereas gradient-based heuristics over-concentrate on edges, leave flat regions underfitting. Conversely, under high-bitrate settings (large  $K$ ), global structure is initially covered, and the extra points will concentrate on high-frequency details to minimize residual error. Therefore, we model the heatmap as a conditional distribution  $\mathcal{H} \sim P(\mathbf{x}|I, K)$ .

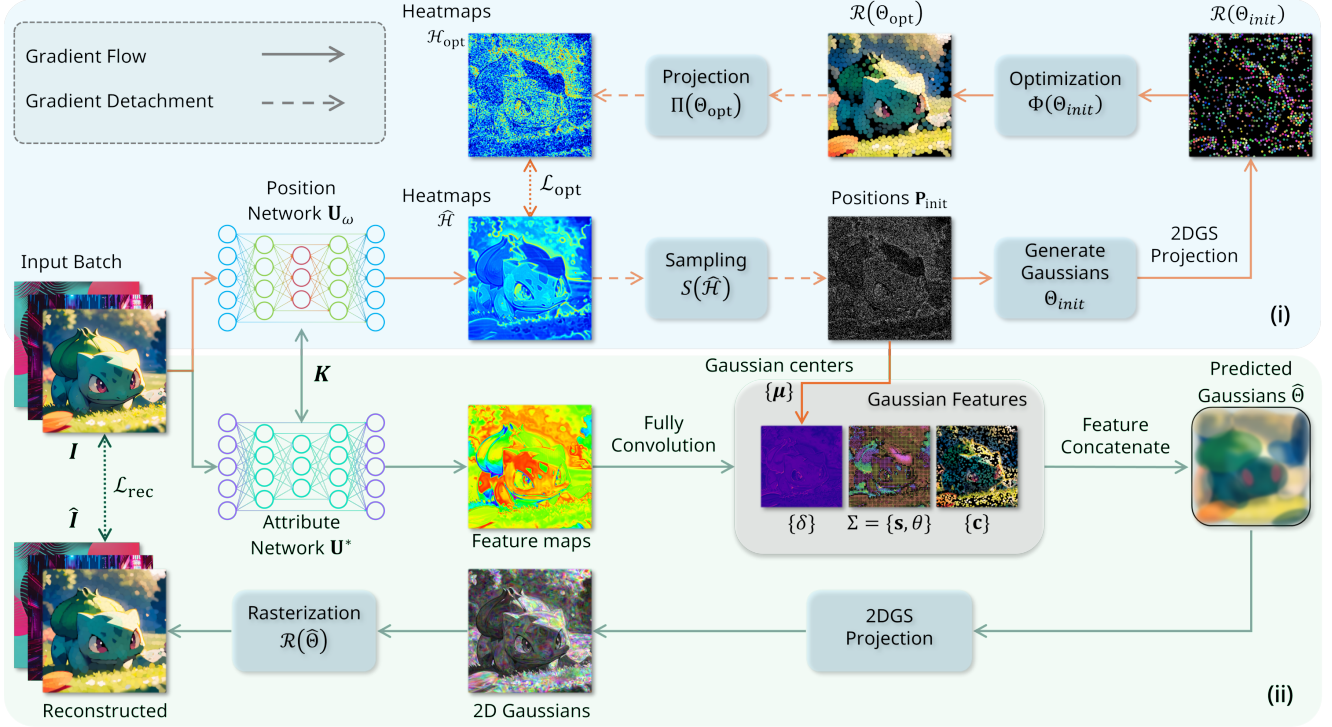


Figure 2. Overview of Fast-2DGS. Taking batch images as input, (i) the Position U-Net first predicts a Heatmap representing the Gaussian Prior, from which initial positions are sampled. (ii) These positions are then combined with predicted features (offsets, scales, rotations, colors) to form full Gaussians for image reconstruction and loss computation.

We employ a lightweight U-Net architecture for Gaussian Prior Heatmap  $\mathcal{H}$  prediction. We inject  $K$  into the network as a global condition to enable dynamic adaptation to varying compression rates. Specifically, we normalize the scalar  $K$  via logarithmic scaling to handle its large dynamic range:

$$\hat{k} = \frac{\log(1 + K)}{\log(1 + K_{\max})}, \quad (6)$$

where  $K_{\max}$  is a predefined upper bound (e.g.,  $10^6$ ). This normalized scalar is then projected into a high-dimensional embedding  $\mathbf{e}_K \in \mathbb{R}^D$  via a learnable MLP.

To modulate the spatial features with  $K$ , we utilize Feature-wise Linear Modulation (FiLM) at the bottleneck [6]. Let  $\mathbf{F} \in \mathbb{R}^{C \times H \times W}$  denote the bottleneck feature map. We compute channel-wise scale  $\gamma \in \mathbb{R}^C$  and shift  $\beta \in \mathbb{R}^C$  vectors from  $\mathbf{e}_K$  to modulate  $\mathbf{F}$  via an affine transformation:

$$\mathbf{F}'_{c,h,w} = \gamma_c(\mathbf{e}_K) \cdot \mathbf{F}_{c,h,w} + \beta_c(\mathbf{e}_K), \quad (7)$$

where the subscripts  $c, h, w$  indicate that the modulation parameters are broadcast across spatial dimensions. The decoder mirrors the encoder structure and outputs the final single-channel probability map  $\mathcal{H}_{pred}$  or  $\hat{\mathcal{H}} \in [0, 1]^{H \times W \times 1}$ .

### 3.4. Bootstrapping Gaussian Initialization

We formulate the Gaussian initialization problem as an iterative bootstrapping learning task: We employ an **Initialization Network**  $\mathbf{U}_\omega$  that generates the initial Gaussian distribution by predicting a spatial probability map  $\hat{\mathcal{H}}$ , and a **Global Optimization Process**  $\Phi$  to optimize the predicted Gaussians subject to reconstruction constraints (e.g., Adam optimization on MSE loss) [15]. Let  $I$  be the input image. The Initialization Network  $\mathbf{U}_\omega$  first predicts a spatial probability distribution  $\hat{\mathcal{H}} = \mathbf{U}_\omega(I)$ . A set of  $K$  initial Gaussian positions, denoted as  $\mathbf{P}_{init}$ , is then sampled from this predicted heatmap:

$$\mathbf{P}_{init} \sim S(\mathbf{U}_\omega(I), K), \quad (8)$$

where  $S(\cdot)$  represents the sampling operation. Specifically, we employ a multinomial sampling strategy in this work [7].

These initial Gaussians are then processed by the gradient-based optimization process  $\Phi(\cdot)$ , as implemented in previous 2D Gaussian Splatting works [41]:

$$\mathbf{P}_{opt} = \Phi(\mathbf{P}_{init}, I). \quad (9)$$

In each training loop, the Global Optimizer provides an optimum target  $\mathcal{H}_{opt}$ . However, since  $\mathbf{P}_{opt}$  is a discrete set,

we apply a projection operator  $\Pi(\cdot)$  to map it back to the continuous domain. The network parameters  $\omega$  are updated to match this target:

$$\mathcal{L}_{opt} = \|\mathcal{H}_{opt} - \hat{\mathcal{H}}\|_2^2, \quad (10)$$

$$= \|\Pi(\mathbf{P}_{opt}) - \mathbf{U}_\omega(I)\|_2^2, \quad (11)$$

While the Initialization Network  $\mathbf{U}_\omega$  initially tends to cluster Gaussians excessively around local high-frequency regions [31], the Global Optimization Process  $\Phi$  generates strong gradients in under-represented regions, forcibly dispersing the Gaussians to minimize the global reconstruction error. Once the prediction of the initialization network aligns with the global optimizer’s stationary distribution, convergence is achieved at a balanced point [16].

### 3.5. Gaussian Attribute Regression

Leveraging the optimized spatial distribution  $\mathbf{P}$  derived from the previous stage as a structural prior, we proceed to regress the remaining Gaussian attributes via a separate U-Net.

While Instant-GI typically samples latent feature vectors and decodes via independent MLP process [37], we predict a single multi-channel tensor  $\mathcal{M} \in \mathbb{R}^{H \times W \times 8}$ , which consists of: **Offset Map** (2 channels) for sub-pixel positional fine-tuning, **Scale Map** (2 channels) for log-space scales, **Color Map** (3 channels) for RGB coefficients, and **Rotation Map** (1 channel) for orientation angles. This fully convolutional design allows for highly efficient, resolution-independent processing.

We reconstruct the final Gaussian set  $\Theta'$  by querying this dense attribute map using the spatial prior  $\mathbf{P}$ . Specifically, for each Gaussian center  $\boldsymbol{\mu}_k = (u_k, v_k) \in \mathbf{P}$ , we sample the corresponding attribute vectors from  $\mathcal{M}$  via grid indexing:

$$\boldsymbol{\delta}_k = \mathcal{M}_{offset}[v_k, u_k], \quad (12)$$

$$\mathbf{s}_k = \mathcal{M}_{scale}[v_k, u_k], \quad (13)$$

$$\theta_k = \mathcal{M}_{rot}[v_k, u_k], \quad (14)$$

$$\mathbf{c}_k = \mathcal{M}_{color}[v_k, u_k]. \quad (15)$$

The Gaussian positions are then refined by adding the learned offsets:  $\boldsymbol{\mu}'_k = \boldsymbol{\mu}_k + \boldsymbol{\delta}_k$ . Finally, we gather all attributes to form the complete Gaussian set:

$$\Theta' = \{\mathbf{g}_k\}_{k=1}^K = \{\boldsymbol{\mu}'_k, \mathbf{s}_k, \mathbf{c}_k, \theta_k\}_{k=1}^K. \quad (16)$$

The collected primitives are rendered via the differentiable rasterization process to produce  $\hat{I}$ . The network is trained end-to-end using the reconstruction loss:

$$\mathcal{L}_{rec} = \|I - \hat{I}\|_2^2 = \|I - \mathcal{R}(\Theta')\|_2^2. \quad (17)$$

## 4. Experiments

### 4.1. Implementation Details

The training is performed on the DIV2K dataset, and the process was divided into two stages using the AdamW optimizer and  $\mathcal{L}_2$  loss. In **Stage I**, the Position Network was trained for 200 epochs ( $\sim 12$  hours) with an initial learning rate of  $5 \times 10^{-4}$ . Crucially, we randomly sampled the primitive budget  $K \sim (10k, 100k)$  during each iteration to enforce complexity-aware initialization. In **Stage II**, we froze the Position Network and train the Attribute Network independently for 500 epochs ( $\sim 7$  hours) with a learning rate of  $1 \times 10^{-4}$  to maximize reconstruction fidelity. Finally, we fine-tune the prediction of rendered images with 5000 iterations ( $\sim 10$  sec) under a learning rate of  $2e-3$  to reach an optimal quality.

### 4.2. Datasets

We evaluate our method on four diverse datasets to ensure comprehensive benchmarking:

- **Kodak PhotoCD Dataset** [39]: A standard benchmark for image reconstruction consisting of 24 lossless, true-color images with a resolution of  $768 \times 512$ . It is widely used to evaluate compression and restoration algorithms.
- **DIV2K Dataset** [1]: A high-quality dataset containing 2K resolution images with diverse real-world content. We utilize the 800 images from the training set for training our models and the 100 images from the validation set for evaluation.
- **Image-GS Stylized Dataset** [41]: To test generalization on non-natural statistics, we adopt the dataset collected by Image-GS, which comprises 45 high-resolution ( $2048 \times 2048$ ) images spanning five categories: vector art, photographs, digital art, anime, and oil painting.
- **Image-GS Texture Dataset** [41]: This dataset contains 19 texture stacks ( $2048 \times 2048$ ) representing various materials (e.g., wood, fabric, metal). This tests the model’s ability to capture high-frequency repetitive patterns crucial for computer graphics workflows.

Since image reconstruction quality is jointly determined by resolution and the primitive count  $K$ , and datasets vary in size, we resized and center-cropped all inputs to a fixed  $512 \times 512$ . This standardization eliminates resolution as a confounding variable, ensuring a fair assessment of the impact of  $K$  across all methods.

### 4.3. Qualitative Analysis

Fig. 3 illustrates the overall pipeline of Fast-2DGS. Given input images, the Position Network predicts a Gaussian Position Prior heatmap (Fig. 3(b)), which is smoother and more continuous than the PPM derived from optimized Gaussian images (Fig. 3(a)), while still capturing different levels of structural details. We then apply Multino-

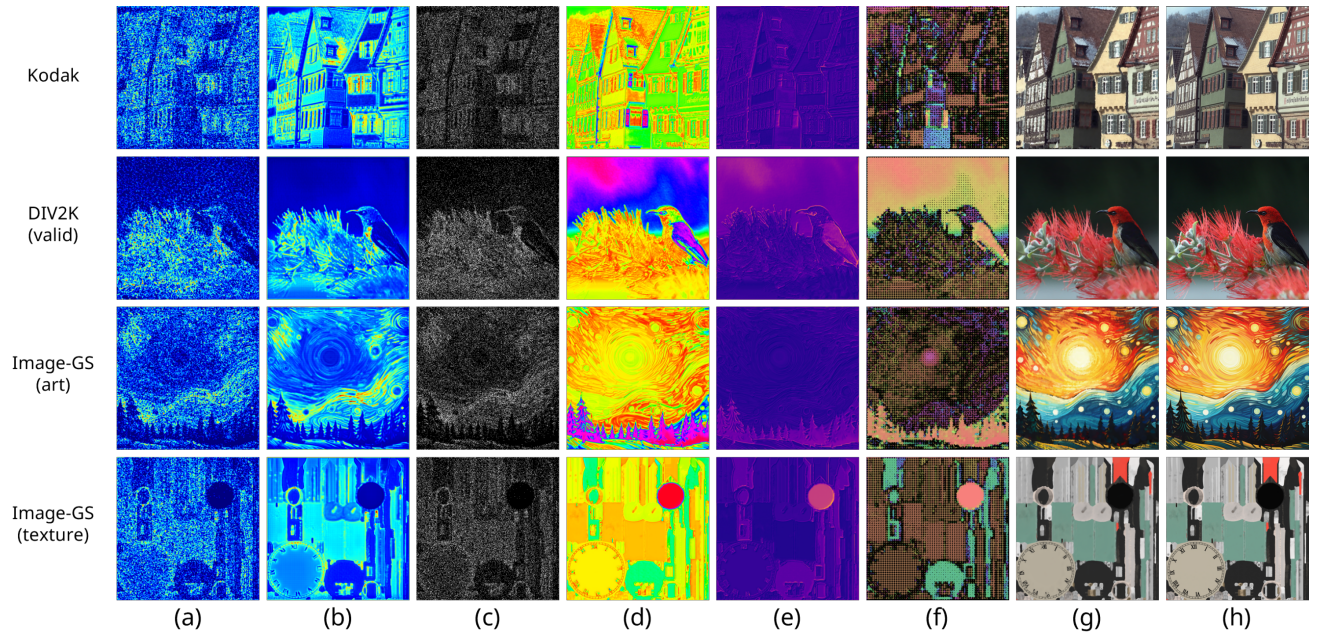


Figure 3. Results of Fast-2DGS. (a) are the reference heatmaps, (b) are the predicted heatmaps from the position network, (c) are the Gaussian positions sampled from the predicted heatmaps, (d) are the feature maps of the last CNN layer, (e) are the offset maps from the attribute network, (f) are the scale-rotation fields, (g) are the predicted Gaussians after rasterization, and (h) are the fine-tuned images.

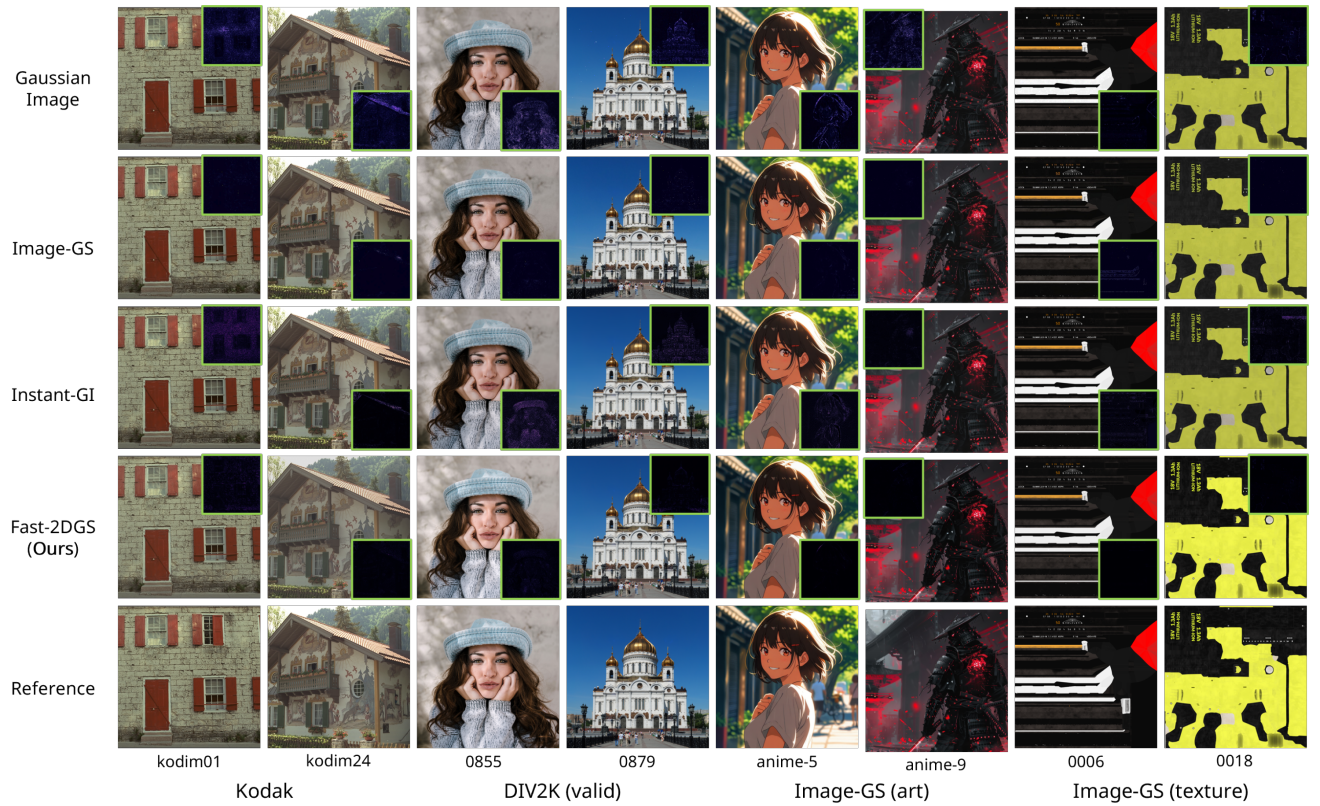


Figure 4. Qualitative comparison against existing Gaussian methods. ROIs represent the error map.

Method	PSNR ↓			MS-SSIM ↓			Time (s) ↓			Training FPS ↑			Latency ↓	Size ↓
	10k	50k	100k	10k	50k	100k	10k	50k	100k	10k	50k	100k		
$K$														
GaussianImage (Cholesky)[39]	19.54	39.36	39.31	0.9685	0.9968	0.9952	12.68	12.85	14.80	2852	2645	2257	-	-
GaussianImage (RS)[39]	30.08	39.78	34.81	0.9684	0.9971	0.9863	13.26	13.66	15.08	2639	2459	2211	-	-
Image-GS (g) [41]	33.26	39.04	39.86	0.9777	0.9939	0.9949	27.76	27.97	30.64	1340	771	508	-	-
Image-GS (s) [41]	34.12	38.65	39.73	0.9835	0.9939	0.9949	22.91	26.48	27.86	1475	777	509	-	-
Instant-GI [37] ( $K=47,246$ )	-	41.41	-	-	0.9960	-	-	10	-	-	-	-	156.39 ms	1172 MB
<b>Fast 2DGS (ours)</b>	33.79	41.85	43.01	0.9865	0.9982	0.9988	5	5	5	-	-	-	4.29 ms	29 MB

Table 1. Benchmark of Gaussian image approaches on the Kodak dataset. We round the results of Instant-GI to 50k level for reference.

mial sampling to select  $K$  Gaussian centers from the predicted heatmap (Fig. 3(c)), enabling effective coverage under limited Gaussian budgets. The sampled positions are used to retrieve corresponding attributes from the Attribute Network (Fig. 3(d)), including offset maps, scale-rotation fields, and color maps. The offset and scale-rotation maps provide sub-pixel positional refinement and shape initialization, respectively. Finally, the predicted Gaussians are rendered by the 2DGS rasterization module to produce an initial reconstruction (Fig. 3(g)), which is further refined with a few fine-tuning steps to obtain the final high-quality result (Fig. 3(h)).

Compared with existing methods, we present qualitative comparisons across four datasets. As shown in Fig. 4, the proposed method achieves visual quality that is comparable to or better than other Gaussian-based approaches, while consistently producing lower reconstruction errors. In particular, our method effectively suppresses artifacts and blurring, demonstrating improved efficiency and robustness across diverse image content.

Method	PSNR ↓			
	Kodak	DIV2K (valid)	ImageGS (art)	ImageGS (texture)
( $K = 50,000$ )				
GaussianImage (Cholesky) [39]	28.19	20.91	28.15	29.09
GaussianImage (RS) [39]	29.20	28.39	28.07	28.90
Image-GS (G) [41]	31.12	27.12	29.21	31.27
Image-GS (S) [41]	30.49	26.80	27.25	29.15
Instant-GI [37]	37.89	38.01	40.38	41.69
<b>Fast 2DGS (ours)</b>	38.14	37.81	41.21	42.51

Table 2. Reconstruction performance comparison across all datasets. Specifically,  $K=50,000$ , and PSNR is calculated at 1st second of fine-tuning.

#### 4.4. Quantitative Results

We primarily evaluate reconstruction quality using Peak Signal-to-Noise Ratio (PSNR) and Multi-Scale Structural Similarity Index (MS-SSIM), where PSNR measures pixel-level reconstruction fidelity, and MS-SSIM captures perceptual and structural similarity across multiple scales [29]. Table 1 reports quantitative comparisons with  $K = 10,000$ , 50,000, and 100,000. In GaussianImage, two covariance parameterizations are considered: Cholesky decomposition and rotation-scaling (RS) decomposition[39]. They are equivalent in representation capacity but differ in optimiza-

tion and compression robustness. While Cholesky performs poorly at low  $K$ , the RS method faces degradation when  $K$  is redundant. For Image-GS, the reported variants (g) and (s) correspond to gradient-based and saliency-based initialization, respectively, representing two heuristic strategies for Gaussian placement. Compared to GaussianImage, Image-GS’s content-adaptive design achieves higher PSNR with more Gaussians. However, both optimization-based methods, while achieving decent PSNR, require longer optimization time and exhibit a clear quality saturation around 40 dB. Instant-GI attains higher reconstruction quality but lacks flexible control over the Gaussian budget, making the compression rate difficult to adjust. In contrast, our method consistently achieves high reconstruction quality with fast runtime while allowing explicit control over  $K$ , providing a better trade-off between quality, efficiency, and flexibility.

Method	PSNR ↓						Total time
	Init.	1s	2s	5s	10s	Final	
( $K = 50,000$ )							
G.Image (Chy.)[39]	13.42	28.19	34.96	38.28	39.20	39.36	13s
G.Image (RS)[39]	13.68	29.31	35.82	38.86	39.62	39.78	14s
Image-GS (g)[41]	27.80	31.12	33.08	34.12	36.19	39.04	28s
Image-GS (S)[41]	27.53	30.49	30.87	33.14	35.78	38.65	28s
Instant-GI[37]	28.26	37.89	39.27	40.60	41.41	41.41	10s
Fast 2DGS (ours)	28.07	38.14	40.05	41.85	43.13	43.13	10s
(w/o Positions)	14.21	31.14	33.50	36.06	39.96	39.96	10s
(w/o Attributes)	10.37	25.07	28.62	32.28	35.69	35.69	10s
(w/o Both)	9.29	27.61	30.07	33.85	35.55	35.55	10s

Table 3. Reconstruction performance on Kodak (average over 24 images).  $K=50,000$ . For Instant-GI,  $K=47,246$ .

Meanwhile, we evaluate the generalizability of all methods. Specifically, we report the PSNR after 1 second of fine-tuning for all methods. As shown in Table 2, our method consistently achieves 37–38 dB PSNR on natural images and exceeds 40 dB PSNR on stylized images and texture datasets.

We further evaluate the convergence speed of different methods during Gaussian image optimization on the Kodak dataset. As shown in Table 3, our method reaches 40 dB PSNR within 2 seconds, whereas other methods require 5 seconds or more to achieve comparable quality. Moreover, our method attains a higher final PSNR, highlighting the importance of effective Gaussian initialization.

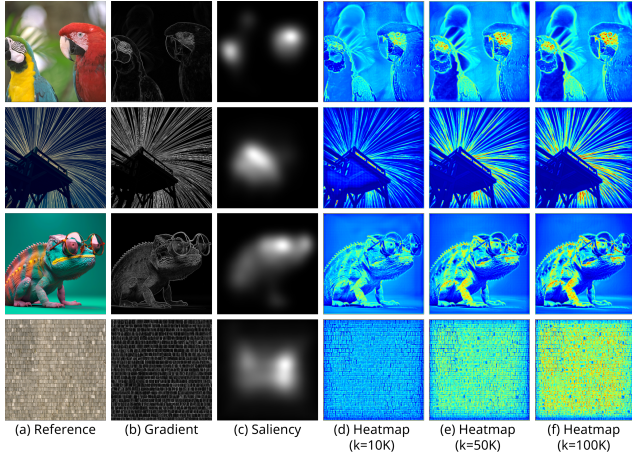


Figure 5. Gaussian initialization comparison. (a) RGB input, (b) Gradient init. (c) Saliency init. (d)(e)(f) Heatmap under  $K$  Gaussians.

#### 4.5. Gaussian Prior Evaluation

To demonstrate the complexity-awareness of our method, we evaluate its behavior under different  $K$ . As shown in Fig. 5, the predicted Gaussian Prior heatmap  $\mathcal{H}_K$  adapts to different values of  $K$  accordingly. When Gaussians are limited, the network encourages a uniform initialization across the image, prioritizing global structure coverage. As  $K$  increases, the network concentrates probability mass on more informative regions, allocating additional Gaussians to detail-rich areas. Compared with heuristic initializations used in Image-GS. The gradient-based initialization, while intuitive, may fail to adequately cover low-frequency areas. The saliency-based initialization successfully captures semantic regions, yet often assigns redundant Gaussians to homogeneous regions.

#### 4.6. Performance and Ablation Studies

**Ablation Analysis** We conduct ablation experiments to analyze the impact of different components in Gaussian initialization, as show in Table 3. When removing the position prediction, the initial reconstruction quality drops to 14 dB PSNR. Nevertheless, due to the preserved attribute initialization, the model is able to recover to 39 dB PSNR after 10 seconds of fine-tuning, still outperforming optimization-based methods. In contrast, when replacing the attributes with random initialization, the initial PSNR further degrades to 10 dB, and the final performance saturates at around 35 dB PSNR even after 10 seconds of optimization. Removing both position and attribute predictions reduces the method to random Gaussian initialization

**Compression Analysis** As shown in Fig. 6, our method supports flexible compression by adjusting  $K$  to arbitrary values. Specifically, with  $K = 50,000$ , the reconstructed image achieves lossless quality, where fine details and textures remain clearly preserved. When  $K$  is reduced to

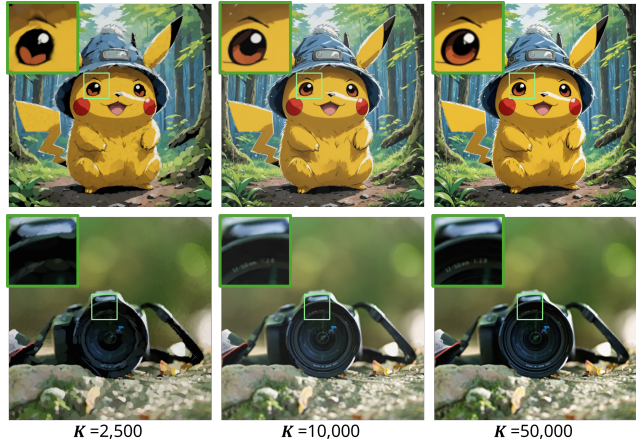


Figure 6. ROIs (Region of Interest) under different  $K$ .

10,000, minor detail loss can be observed, yet the overall visual quality remains high and perceptually faithful. Under more aggressive compression ( $K = 2,500$ ), fine-grained details, particularly structured textures such as text, begin to vanish; however, the global semantic structure is largely preserved, and no severe blurring or smearing artifacts are introduced. These results demonstrate that our representation degrades gracefully under compression, retaining semantic integrity even at very limited Gaussian primitives.

**Computation Analysis** Both our method and Instant-GI adopt network predictions followed by a fine-tuning process. In terms of network inference latency, our method requires only 4.29 ms, whereas Instant-GI incurs a significantly higher cost of 156.39 ms, as shown in Table 1. Moreover, Instant-GI relies on a heavy network with a weight size of 1,172 MB, while our two lightweight networks together occupy only 29 MB in total (14.68 MB + 14.82 MB). This substantial reduction in latency and model size makes our design more suitable for practical tasks.

## 5. Conclusion

We conclude that the training of Gaussian images is heavily dependent on initialization, and we demonstrate that initialization priors can be effectively modeled by deep learning. Experiments on four representative datasets show that it requires no extensive feature engineering and heavy computation resources to achieve state-of-the-art performance, but a simple neural network. However, while we believe our approach paves the way for the next generation of image codecs, this is only the inception of Gaussian image representation. Despite low latency, our current network design may bottleneck performance on high-resolution images (e.g., 4K/8K). That said, Gaussian image representation still has a long way to meet industry standards for real-time, end-to-end compression required in the AIGC era. Therefore, our future work will explore scalable learning and explicit feature learning in generative models to close this gap.

## References

- [1] Eirikur Agustsson and Radu Timofte. Ntire 2017 challenge on single image super-resolution: Dataset and study. In *The IEEE Conference on Computer Vision and Pattern Recognition (CVPR) Workshops*, 2017. 5
- [2] Saeed Anwar and Nick Barnes. Densely residual laplacian super-resolution. *IEEE Transactions on Pattern Analysis and Machine Intelligence*, 44(3):1192–1204, 2020. 2
- [3] Arpit Bansal, Eitan Borgnia, Hong-Min Chu, Jie Li, Hamid Kazemi, Furong Huang, Micah Goldblum, Jonas Geiping, and Tom Goldstein. Cold diffusion: Inverting arbitrary image transforms without noise. *Advances in Neural Information Processing Systems*, 36, 2024. 2
- [4] Wenbo Bao, Wei-Sheng Lai, Xiaoyun Zhang, Zhiyong Gao, and Ming-Hsuan Yang. Memc-net: Motion estimation and motion compensation driven neural network for video interpolation and enhancement. *IEEE transactions on pattern analysis and machine intelligence*, 43(3):933–948, 2019. 1
- [5] Ashish Bastola, Nishant Luitel, Hao Wang, Danda Pani Paudel, Roshani Poudel, and Abolfazl Razi. Robustformer: Noise-robust pre-training for images and videos. *arXiv preprint arXiv:2411.13040*, 2024. 2
- [6] Sawyer Birnbaum, Volodymyr Kuleshov, Zayd Enam, Pang Wei W Koh, and Stefano Ermon. Temporal film: Capturing long-range sequence dependencies with feature-wise modulations. *Advances in Neural Information Processing Systems*, 32, 2019. 4
- [7] Saul Blumenthal. Multinomial sampling with partially categorized data. *Journal of the American Statistical Association*, 63(322):542–551, 1968. 4
- [8] Yihang Chen, Qianyi Wu, Mehrtash Harandi, and Jianfei Cai. How far can we compress instant-ngp-based nerf? In *Proceedings of the IEEE/CVF Conference on Computer Vision and Pattern Recognition*, pages 20321–20330, 2024. 1, 2
- [9] Renato J Cintra and Fábio M Bayer. A dct approximation for image compression. *IEEE Signal Processing Letters*, 18(10):579–582, 2011. 2
- [10] Jiajun Dong, Chengkun Wang, Wenzhao Zheng, Lei Chen, Jiwen Lu, and Yansong Tang. Gaussian token: An effective image tokenizer with 2d gaussian splatting. *arXiv preprint arXiv:2501.15619*, 2025. 1
- [11] Xuanzhao Dong, Vamsi Krishna Vasa, Wenhui Zhu, Peijie Qiu, Xiwen Chen, Yi Su, Yujian Xiong, Zhangsihao Yang, Yanxi Chen, and Yalin Wang. Cunsb-rfie: Context-aware unpaired neural schrödinger bridge in retinal fundus image enhancement. In *2025 IEEE/CVF Winter Conference on Applications of Computer Vision (WACV)*, pages 4502–4511. IEEE, 2025. 3
- [12] Emilien Dupont, Hrushikesh Loya, Milad Alizadeh, Adam Goliński, Yee Whye Teh, and Arnaud Doucet. Coin++: Neural compression across modalities. *arXiv preprint arXiv:2201.12904*, 2022. 2
- [13] Lakshya Gupta and Imran N Junejo. Neural video compression using 2d gaussian splatting. *arXiv preprint arXiv:2505.09324*, 2025. 1
- [14] Feihong He, Gang Li, Mengyuan Zhang, Leilei Yan, Lingyu Si, and Fanzhang Li. Freestyle: Free lunch for text-guided style transfer using diffusion models. *arXiv preprint arXiv:2401.15636*, 2024. 1, 2
- [15] Chih-Hui Ho and Nuno Vasconcelos. Disco: Adversarial defense with local implicit functions. *Advances in neural information processing systems*, 35:23818–23837, 2022. 4
- [16] Ya-Ping Hsieh, Chen Liu, and Volkan Cevher. Finding mixed nash equilibria of generative adversarial networks. In *International Conference on Machine Learning*, pages 2810–2819. PMLR, 2019. 5
- [17] Jintong Hu, Bin Xia, Bin Chen, Wenming Yang, and Lei Zhang. Gaussiansr: High fidelity 2d gaussian splatting for arbitrary-scale image super-resolution. In *Proceedings of the AAAI Conference on Artificial Intelligence*, pages 3554–3562, 2025. 2
- [18] Thomas S Huang. Digital holography. *Proceedings of the IEEE*, 59(9):1335–1346, 1971. 3
- [19] Juho Lee, Yoonho Lee, Jungtaek Kim, Adam Kosior, Seungjin Choi, and Yee Whye Teh. Set transformer: A framework for attention-based permutation-invariant neural networks. In *International conference on machine learning*, pages 3744–3753. PMLR, 2019. 3
- [20] Yue Li, Qi Ma, Runyi Yang, Huapeng Li, Mengjiao Ma, Bin Ren, Nikola Popovic, Nicu Sebe, Ender Konukoglu, Theo Gevers, et al. Scenesplat: Gaussian splatting-based scene understanding with vision-language pretraining. *arXiv preprint arXiv:2503.18052*, 2025. 2
- [21] Haotong Lin, Sili Chen, Junhao Liew, Donny Y Chen, Zhenyu Li, Guang Shi, Jiashi Feng, and Bingyi Kang. Depth anything 3: Recovering the visual space from any views. *arXiv preprint arXiv:2511.10647*, 2025. 2
- [22] Junmin Liu, Yijun Chen, Jianshe Zhang, and Zongben Xu. Enhancing low-rank subspace clustering by manifold regularization. *IEEE Transactions on Image Processing*, 23(9):4022–4030, 2014. 3
- [23] Xi Liu, Chaoyi Zhou, and Siyu Huang. 3dgs-enhancer: Enhancing unbounded 3d gaussian splatting with view-consistent 2d diffusion priors. *Advances in Neural Information Processing Systems*, 37:133305–133327, 2024. 2
- [24] Wenxuan Lu, Jiangyang He, Zhanqiu Zhang, Steven Y Guo, and Tianning Zang. Cultivating gaming sense for yourself: Making vlms gaming experts. In *Proceedings of the 63rd Annual Meeting of the Association for Computational Linguistics (Volume 1: Long Papers)*, pages 13132–13152, 2025. 1
- [25] Balas Kausik Natarajan. Sparse approximate solutions to linear systems. *SIAM journal on computing*, 24(2):227–234, 1995. 3
- [26] Qian Ning, Weisheng Dong, Xin Li, Jinjian Wu, and Guangming Shi. Uncertainty-driven loss for single image super-resolution. *Advances in Neural Information Processing Systems*, 34:16398–16409, 2021. 3
- [27] Stephen M Omohundro. “floyd-steinberg dithering. In *Proceedings of International Conference on Computer Science*, pages 1–12, 1947. 2
- [28] Jeongsoo Park and Justin Johnson. Rgb no more: Minimally-decoded jpeg vision transformers. In *Proceedings of the*

- IEEE/CVF Conference on Computer Vision and Pattern Recognition*, pages 22334–22346, 2023. 1
- [29] Thomas Richter and Kil Joong Kim. A ms-ssim optimal jpeg 2000 encoder. In *2009 Data Compression Conference*, pages 401–410. IEEE, 2009. 7
- [30] Vishwanath Saragadam, Daniel LeJeune, Jasper Tan, Guha Balakrishnan, Ashok Veeraraghavan, and Richard G Baraniuk. Wire: Wavelet implicit neural representations. In *Proceedings of the IEEE/CVF Conference on Computer Vision and Pattern Recognition*, pages 18507–18516, 2023. 2
- [31] Chenyang Si, Ziqi Huang, Yuming Jiang, and Ziwei Liu. Freeu: Free lunch in diffusion u-net. In *Proceedings of the IEEE/CVF Conference on Computer Vision and Pattern Recognition*, pages 4733–4743, 2024. 5
- [32] Vincent Sitzmann, Julien Martel, Alexander Bergman, David Lindell, and Gordon Wetzstein. Implicit neural representations with periodic activation functions. *Advances in neural information processing systems*, 33:7462–7473, 2020. 2
- [33] Yannick Strümler, Janis Postels, Ren Yang, Luc Van Gool, and Federico Tombari. Implicit neural representations for image compression. In *European Conference on Computer Vision*, pages 74–91. Springer, 2022. 1, 2
- [34] Joanna Waczyńska, Tomasz Szczepanik, Piotr Borycki, Sławomir Tadeja, Thomas Bohné, and Przemysław Spurek. Mirage: Editable 2d images using gaussian splatting. *arXiv preprint arXiv:2410.01521*, 2024. 1
- [35] Hao Wang, Jiayou Qin, Xiwen Chen, Ashish Bastola, John Suchanek, Zihao Gong, and Abolfazl Razi. Motor focus: Fast ego-motion prediction for assistive visual navigation. In *2024 IEEE 20th International Conference on Body Sensor Networks (BSN)*, pages 1–4. IEEE, 2024. 2
- [36] Jiacong Xu, Yiqun Mei, and Vishal Patel. Wild-gs: Real-time novel view synthesis from unconstrained photo collections. *Advances in Neural Information Processing Systems*, 37:103334–103355, 2024. 2
- [37] Zhaojie Zeng, Yuesong Wang, Tao Guan, Chao Yang, and Lili Ju. Instant gaussianimage: A generalizable and self-adaptive image representation via 2d gaussian splatting. In *Proceedings of the IEEE/CVF International Conference on Computer Vision*, pages 27896–27905, 2025. 2, 3, 5, 7
- [38] Yu-Ting Zhan, He-bi Yang, Cheng-Yuan Ho, Jui-Chiu Chiang, and Wen-Hsiao Peng. Cat-3dgs pro: A new benchmark for efficient 3dgs compression. *arXiv preprint arXiv:2503.12862*, 2025. 2
- [39] Xinjie Zhang, Xingtong Ge, Tongda Xu, Dailan He, Yan Wang, Hongwei Qin, Guo Lu, Jing Geng, and Jun Zhang. Gaussianimage: 1000 fps image representation and compression by 2d gaussian splatting. In *European Conference on Computer Vision*, pages 327–345. Springer, 2024. 1, 2, 5, 7
- [40] Xinxi Zhang, Song Wen, Ligong Han, Felix Juefei-Xu, Akash Srivastava, Junzhou Huang, Vladimir Pavlovic, Hao Wang, Molei Tao, and Dimitris Metaxas. Soda: Spectral orthogonal decomposition adaptation for diffusion models. In *2025 IEEE/CVF Winter Conference on Applications of Computer Vision (WACV)*, pages 4665–4682. IEEE, 2025. 1, 2
- [41] Yunxiang Zhang, Bingxuan Li, Alexandr Kuznetsov, Akshay Jindal, Stavros Diolatzis, Kenneth Chen, Anton Sochenov, Anton Kaplanyan, and Qi Sun. Image-gs: Content-adaptive image representation via 2d gaussians. In *Proceedings of the Special Interest Group on Computer Graphics and Interactive Techniques Conference Conference Papers*, pages 1–11, 2025. 1, 2, 3, 4, 5, 7
- [42] Shihao Zhao, Dongdong Chen, Yen-Chun Chen, Jianmin Bao, Shaozhe Hao, Lu Yuan, and Kwan-Yee K Wong. Uni-controlnet: All-in-one control to text-to-image diffusion models. *Advances in Neural Information Processing Systems*, 36, 2024. 1
- [43] Zixiang Zhao, Jianshe Zhang, Shuang Xu, Zudi Lin, and Hanspeter Pfister. Discrete cosine transform network for guided depth map super-resolution. In *Proceedings of the IEEE/CVF conference on computer vision and pattern recognition*, pages 5697–5707, 2022. 2
- [44] Chaoyi Zhou, Xi Liu, Feng Luo, and Siyu Huang. Latent radiance fields with 3d-aware 2d representations. In *The Thirteenth International Conference on Learning Representations*. 2
- [45] Lingting Zhu, Guying Lin, Jinnan Chen, Xinjie Zhang, Zhenchao Jin, Zhao Wang, and Lequan Yu. Large images are gaussians: High-quality large image representation with levels of 2d gaussian splatting. In *Proceedings of the AAAI Conference on Artificial Intelligence*, pages 10977–10985, 2025. 1